ATLAS NOTE

ATLAS-CONF-2012-003

February 12, 2012

Search for supersymmetry in pp collisions at $\sqrt{s} = 7$ TeV in final states with missing transverse momentum and b-jets with the ATLAS detector

The ATLAS Collaboration

ATLAS-CONF-2012-003
14 February 2012

Abstract

The results of a search for supersymmetry in events with large missing transverse momentum and heavy flavour jets using an integrated luminosity corresponding to 2.05 fb^{-1} of pp collisions at $\sqrt{s} = 7$ TeV recorded with the ATLAS detector are reported. No significant excess is observed with respect to the prediction for Standard Model processes. Results are interpreted in a variety of R-parity conserving models in which scalar bottoms and tops are the only scalar quarks to appear in the gluino decay cascade, and in an SO(10) model framework. Gluino masses up to 600–900 GeV are excluded, depending on the model considered.

1 Introduction

Supersymmetry (SUSY) [1–9] is a framework that provides an extension of the Standard Model (SM) and naturally resolves the hierarchy problem [10,11] by introducing supersymmetric partners of the known bosons and fermions. In the MSSM, which is an R-parity conserving minimal supersymmetric extension of the SM, SUSY particles are produced in pairs and the lightest supersymmetric particle (LSP) is stable, providing a possible candidate for dark matter. In a large variety of models, the LSP is the lightest neutralino, $\tilde{\chi}_1^0$. The coloured superpartners of quarks and gluons, the squarks ($\tilde{q}$) and gluinos ($\tilde{g}$), are expected to be produced in strong interaction processes at the centre-of-mass energy of the Large Hadron Collider (LHC). Their decays via cascades ending with the LSP would produce striking experimental signatures leading to final states containing multiple jets, missing transverse momentum (its magnitude is referred to as $E_{\mathrm{T}}^{\mathrm{miss}}$ in the following) – resulting from the undetected neutralinos – and possibly leptons. In the MSSM, the scalar partners of right-handed and left-handed quarks, $\tilde{q}_R$ and $\tilde{q}_L$, can mix to form two mass eigenstates. The mixing effect is proportional to the corresponding SM fermion masses and therefore becomes important for the third generation. Large mixing can yield scalar bottom (sbottom, $\tilde{b}_1$) and scalar top (stop, $\tilde{t}_1$) mass eigenstates which are significantly lighter than other squarks. Consequently, $\tilde{b}_1$ and $\tilde{t}_1$ could be produced with large cross sections at the LHC, either directly in pairs, or through $\tilde{g}\tilde{g}$ production with subsequent $\tilde{g} \to \tilde{b}_1 b$ or $\tilde{g} \to \tilde{t}_1 t$ decays (gluino-mediated production).

In this note, a search for scalar top and bottom quarks using an integrated luminosity corresponding to 2.05 fb^{-1} of $\sqrt{s} = 7$ TeV proton-proton collisions at the LHC, is presented. Events are selected by requiring large $E_{\mathrm{T}}^{\mathrm{miss}}$, several jets, including b-quark jets (b-jets), and either vetoing (0-lepton channel) or requiring (1-lepton channel) charged leptons. The search is mostly sensitive to the gluino-mediated production of third generation squarks. Results are interpreted in the framework of various simplified models in which scalar bottoms and tops are the only squarks that appear in the gluino decay cascade, and in specific Grand Unification Theories (GUTs) based on the gauge group SO(10) [12, 13].

The note is an update of a search presented by the ATLAS collaboration using 35 pb^{-1} of data collected in 2010 [14], with a number of improvements. The analysis has been extended by including more signal regions which profit from the increased available integrated luminosity and maximise the sensitivity to a large variety of SUSY scenarios. Data-driven methods are employed to estimate the contributions of SM background processes. Searches for scalar bottom quarks via $\tilde{g}\tilde{g}$ production have been also reported by the CMS [15] collaboration. Searches sensitive to direct scalar bottom production irrespective of gluino mass have been published by the ATLAS collaboration [16] using the same data-set employed in this paper.

2 The ATLAS detector

The ATLAS detector [17] comprises an inner detector surrounded by a thin superconducting solenoid and a calorimeter system. Outside the calorimeters is an extensive muon spectrometer in a toroidal magnetic field.

The inner detector system is immersed in a 2 T axial magnetic field and provides tracking information for charged particles in a pseudorapidity range $|\eta| < 2.5$ [1]. The highest granularity is achieved around the vertex region using silicon pixel and microstrip (SCT) detectors. These

[1] The azimuthal angle ϕ is measured around the beam axis and the polar angle θ is the angle from the beam axis. The pseudorapidity is defined as $\eta = -\ln\tan(\theta/2)$. The distance ΔR in the $\eta - \phi$ space is defined as $\Delta R = \sqrt{(\Delta\eta)^2 + (\Delta\phi)^2}$.

detectors allow for an efficient tagging of jets originating from b-quark decays using impact parameter measurements and the reconstruction of secondary decay vertices. The transition radiation tracker (TRT), which surrounds the silicon detectors, contributes to track reconstruction up to $|\eta| = 2.0$ and improves the electron identification by the detection of transition radiation.

The calorimeter system covers the pseudorapidity range $|\eta| < 4.9$. The highly-segmented electromagnetic calorimeter consists of lead absorbers with liquid argon (LAr) as the active material and covers the pseudorapidity range $|\eta| < 3.2$. In the region $|\eta| < 1.8$, a pre-sampler detector using a thin layer of liquid argon is used to correct for the energy lost by electrons and photons upstream of the calorimeter. The hadronic tile calorimeter is a steel/scintillating-tile detector and is situated directly outside the envelope of the electromagnetic calorimeter. Two hadronic end-cap calorimeters with liquid argon as active material and copper or tungsten as absorber material are used in the forward region.

Muon detection is based on the magnetic deflection of muon tracks in the large superconducting air-core toroid magnets, instrumented with separate trigger and high-precision tracking chambers. A system of three eight-coils toroids, a barrel and two end-caps, generates the magnetic field for the muon spectrometer in the pseudorapidity range $|\eta| < 2.7$.

3 Monte Carlo simulation

Simulated event samples are used to aid in the description of the background and to model the SUSY signal. Top quark pair and single top quark production are simulated with `MC@NLO` [18], fixing the top quark mass at 172.5 GeV, and using the next-to-leading-order (NLO) parton density function (PDF) set `CTEQ6.6` [19]. Additional Monte Carlo (MC) samples generated with `POWHEG` [20] and `ACERMC` [21] are used to estimate the event generator systematic uncertainties. Samples of W+jets, Z+jets with light and heavy flavour jets, and $t\bar{t}$ with additional b-jets, $t\bar{t}b\bar{b}$, are generated with `ALPGEN` [22] and the PDF set `CTEQ6L1` [23]. The fragmentation and hadronisation for the `ALPGEN` and `MC@NLO` samples are performed with `HERWIG` [24], using `JIMMY` [25] for the underlying event. Samples of $Zt\bar{t}$ and $Wt\bar{t}$ are generated with `MADGRAPH` [26] interfaced to `PYTHIA` [27]. Di-boson (WW, WZ, ZZ) samples are generated with `HERWIG`. The signal samples are generated using the `HERWIG++` [28] v2.4.2 Monte Carlo program. The SUSY sample yields are normalised to the results of NLO calculations, as obtained using the `PROSPINO` [29] v2.1 program and the parameterisation of the PDFs is done with `CTEQ6.6M` [30]. The MC samples are produced using parameters tuned as described in [31] and are processed through a detector simulation [32] based on `GEANT4` [33]. Effects of multiple proton-proton interactions per bunch crossing are included in the simulation, and MC events are reweighted to reproduce the mean expected number of collisions per bunch crossing estimated for data.

The background predictions, obtained from theoretical cross sections, including higher-order QCD corrections when available, are compared to data in control regions. The cross sections times branching ratio in the relevant final states used for each Standard Model background process are listed in Table 1. The W and Z/γ^* production processes are normalised to the next-to-next-to-leading order (NNLO) cross sections while the $t\bar{t}$ and single top production are normalised to the NLO+NNLL (next-to-next-to-leading logarithms) cross sections. The normalisation of the di-boson production is based on cross sections determined at NLO using MCFM [34, 35]. The $t\bar{t}$ production in association with W/Z or $b\bar{b}$ is normalised to LO and a conservative uncertainty of 100% is assumed.

For background from QCD jet production processes (multi-jet in the following), no reliable prediction can be obtained from a leading-order Monte Carlo simulation and data-driven methods are used to determine the residual contributions of this background to the selected

Physics process	$\sigma \cdot$ BR [nb] (perturbative order)	
$W \to \ell\nu$	31.4 (NNLO)	[36–38]
$Z/\gamma^* \to \ell^+\ell^-$	3.20 (NNLO)	[36–38]
$Z \to \nu\bar{\nu}$	5.82 (NNLO)	[36–38]
$t\bar{t}$	0.165 (NLO+NNLL)	[39–41]
Single top	0.085 (NLO+NNLL)	[39–41]
$t\bar{t}b\bar{b}$	0.9×10^{-3} (LO)	[22]
$t\bar{t}$+W/Z	0.4×10^{-3} (LO)	[26]
WW, WZ, ZZ	0.071 (NLO)	[34, 35]

Table 1: The most important background processes and their production cross sections, multiplied by the relevant branching ratios (BR). The ℓ indicates all three types of leptons (e, μ, τ) summed together. Contributions from higher order QCD corrections are included for W and Z boson production (NNLO corrections), for $t\bar{t}$ production (NLO+NNLL corrections) and for di-boson production (NLO corrections). The $Z/\gamma^* \to \ell^+\ell^-$ cross section is given for events with a di-lepton invariant mass of at least 40 GeV. The cross-sections for $t\bar{t}b\bar{b}$ and $t\bar{t}$+W/Z production are given at leading order (LO).

event samples, as discussed in Section 6.

4 Object reconstruction

Electrons are reconstructed from energy clusters in the electromagnetic calorimeter matched to a track in the inner detector. They are selected using the "medium" [42] selection based on calorimeter shower shape, inner-detector track quality, and track-to-calorimeter cluster matching. The "medium" electron selection is used to estimate the contribution from non-isolated and mis-identified electrons, and when a veto on additional electrons is required. Electrons used in the final selection are required to pass the "tight" electron definition, which adds a requirement on the ratio E/p between the calorimeter cluster energy E and the track momentum p, and on detection of transition radiation in the TRT. Furthermore, the electron is required to be isolated: the scalar transverse momentum (p_{T}) sum of tracks within a cone in the η, ϕ plane of radius $\Delta R = 0.2$ around the electron candidate, $\Sigma_{p_{\mathrm{T}}}$, must be less than 10% of the electron p_{T}. Medium electrons are required to pass kinematic requirements of $p_{\mathrm{T}} > 20$ GeV and $|\eta| < 2.47$, while the p_{T} threshold is raised to 25 GeV for tight electrons. In addition, electrons with a distance to the closest jet of $0.2 < \Delta R < 0.4$ are discarded.

Muons are identified as a match between an extrapolated inner detector track and one or more track segments in the muon spectrometer. The inner detector track must have at least two hits in the pixel detector (one of which is required to be in the innermost layer), at least six hits in the SCT, and fewer than two missing hits on the track in the pixel and SCT detectors. For $|\eta| < 1.9$, at least six TRT hits are required. Muons with a distance to the closest jet of $\Delta R < 0.4$ are discarded. In order to reject muons resulting from cosmic rays, tight criteria are applied on the proximity of the muon trajectories to the primary vertex (PV): $|z_\mu - z_{PV}| < 1$ mm and $|d_0| < 0.2$ mm, where z_μ is the z coordinate of the extrapolated muon track at the point of closest approach to the PV, z_{PV} is the coordinate of the PV, and $|d_0|$ is the magnitude of the impact parameter of the muon in the transverse plane. These pre-selected muons, satisfying $p_{\mathrm{T}} > 10$ GeV and $|\eta| < 2.4$, are used to quantify the contribution from non-isolated muons and when a veto on additional muons is required. For muons in the final selection, the p_{T}

requirement is raised to 20 GeV and the muon is required to be isolated with $\Sigma_{p_T} < 1.8$ GeV.

Jets are reconstructed from three-dimensional calorimeter energy clusters by using the anti-k_t jet algorithm [43, 44] with a radius parameter of 0.4. The measured jet energy is corrected for inhomogeneities and for the non-compensating nature of the calorimeter by using p_T- and η-dependent correction factors [45]. Jets are required to have $p_T > 20$ GeV and $|\eta| < 2.8$. Events with jets not passing jet quality criteria against noise and non-collision backgrounds are rejected. The quality criteria used are the same as in Ref. [45]. Additionally, in the 0-lepton channel the three leading jets, if central ($|\eta| < 2$), are required to have a jet charged fraction (defined as the scalar sum of the transverse momenta of the tracks associated to the jet divided by the jet p_T) of at least 5%. Jets within a distance of $\Delta R < 0.2$ of a pre-selected electron are rejected, since these jets are likely to be electrons also reconstructed as jets. For jets in the signal regions, the p_T requirement is tightened to 50 GeV to remove jets that are not associated with the hard scattering of interest.

A b-tagging algorithm exploiting both impact parameter and secondary vertex information [46] is used to identify jets containing a b-hadron decay. This algorithm has a 60% efficiency for tagging b-jets in a MC sample of $t\bar{t}$ events, with a mis-tag rate for light quarks and gluons of less than 1%. These b-jets are identified within the nominal acceptance of the inner detector ($|\eta| < 2.5$) and they are required to have $p_T > 50$ GeV.

The calculation of E_T^{miss} [47] is based on the modulus of the vectorial sum of the p_T of the reconstructed jets (with $p_T > 20$ GeV and $|\eta| < 4.5$), pre-selected leptons — including non-isolated muons — and calorimeter clusters not belonging to other reconstructed objects.

During a fraction of the data-taking period (about 40% of the total integrated luminosity), a localised electronics failure in the LAr barrel calorimeter created a dead region in the second and third calorimeter layers ($\Delta\eta \times \Delta\phi \simeq 1.4 \times 0.2$) in which on average 30% of the incident jet energy is not measured. Negligible impact is found on the reconstruction efficiency for jets with $p_T > 20$ GeV. For events selected during this data period, if any jet with $p_T > 50$ GeV falls in the aforementioned region, the event is rejected. The loss in signal acceptance is smaller than 10% in the affected period for the models considered.

In the event selection, a number of variables derived from the reconstructed objects are used. The transverse mass m_T formed by E_T^{miss} and the p_T of the lepton is defined as:

$$m_T = \sqrt{2p_T^{lep}E_T^{miss} - 2\vec{\mathbf{p}}_T^{lep} \cdot \vec{\mathbf{E}}_T^{miss}} \quad (1)$$

The effective mass m_{eff} is obtained as the scalar p_T sum of all selected objects in the event:

$$m_{eff} = \sum_{i \leq n} (p_T^{jet})_i + E_T^{miss} + \sum_j (p_T^{lep})_j \quad (2)$$

where n corresponds to the number of jets used in a given signal region.

The minimum azimuthal separation between the n selected jets in a given signal region and the E_T^{miss} direction ($\Delta\phi_{min}$) is defined as:

$$\Delta\phi_{min} = \min(|\phi_1 - \phi_{E_T^{miss}}|, ..., |\phi_n - \phi_{E_T^{miss}}|) \quad (3)$$

where the index refers to the p_T-ordered list of jets.

5 Event Selection

This search uses proton-proton collisions recorded from March to August 2011 at a centre-of-mass energy of 7 TeV. After the application of beam, detector and data quality requirements,

the data set consists of a total integrated luminosity of 2.05 ± 0.08 fb^{-1} [48, 49]. Two groups of signal regions are defined based on the presence of a charged lepton ($\ell = e, \mu$) in the final state and are further referred to as 0-lepton and 1-lepton channels. In the 0-lepton channel, a veto on pre-selected leptons is applied, while exactly one lepton is required in the 1-lepton channel. Events containing two or more leptons are the subject of a different study [50].

The data are selected with a three-level trigger system. A trigger requiring a high transverse momentum jet and missing transverse momentum is used to select events for the 0-lepton channel. The plateau efficiency is reached for jets with $p_{\mathrm{T}} > 130$ GeV and $E_{\mathrm{T}}^{\mathrm{miss}} > 130$ GeV. A single electron trigger, reaching the plateau efficiency for offline electrons with $p_{\mathrm{T}} \geq 25$ GeV, and a combined muon-jet trigger, reaching the plateau efficiency for muons with $p_{\mathrm{T}} \geq 20$ GeV and jets with $p_{\mathrm{T}} \geq 60$ GeV are used for the 1-lepton channel.

Events are required to have a reconstructed primary vertex associated with five or more tracks with $p_{\mathrm{T}} > 0.4$ GeV, and must pass basic quality criteria against detector noise and non-collision backgrounds.

For the 0-lepton selection, at least one jet with $p_{\mathrm{T}} > 130$ GeV, at least two additional jets with $p_{\mathrm{T}} > 50$ GeV and $E_{\mathrm{T}}^{\mathrm{miss}} > 130$ GeV are required. At least one of the selected jets is required to be b-tagged. To reduce the amount of multi-jet background, where $E_{\mathrm{T}}^{\mathrm{miss}}$ results from mis-reconstructed jets or from neutrinos emitted close to the direction of the jet axis, additional cuts of $\Delta\phi_{\mathrm{min}} > 0.4$ and $E_{\mathrm{T}}^{\mathrm{miss}}/m_{\mathrm{eff}} > 0.25$ are applied.

Pre-selection	Signal Region name	Selection
no leptons, at least three jets, $p_{\mathrm{T}}(j1) > 130$ GeV, $p_{\mathrm{T}}(j2, j3) > 50$ GeV, $E_{\mathrm{T}}^{\mathrm{miss}} > 130$ GeV, $E_{\mathrm{T}}^{\mathrm{miss}}/m_{\mathrm{eff}} > 0.25$, $\Delta\phi_{\mathrm{min}} > 0.4$, at least one b-tag	SR0-A1	$m_{\mathrm{eff}} > 500$ GeV
	SR0-B1	$m_{\mathrm{eff}} > 700$ GeV
	SR0-C1	$m_{\mathrm{eff}} > 900$ GeV
	SR0-A2	two b-tags, $m_{\mathrm{eff}} > 500$ GeV
	SR0-B2	two b-tags, $m_{\mathrm{eff}} > 700$ GeV
	SR0-C2	two b-tags, $m_{\mathrm{eff}} > 900$ GeV
one lepton, at least four jets $p_{\mathrm{T}}(j1) > 60$ GeV, $p_{\mathrm{T}}(j2, j3, j4) > 50$ GeV, $E_{\mathrm{T}}^{\mathrm{miss}} > 80$ GeV, $m_{\mathrm{T}} > 100$ GeV, at least one b-tag	SR1-D	$m_{\mathrm{eff}} > 700$ GeV
	SR1-E	$m_{\mathrm{eff}} > 700$ GeV, $E_{\mathrm{T}}^{\mathrm{miss}} > 200$ GeV

Table 2: Signal regions definition for the 0-lepton and 1-lepton channels. The first column summarises the common pre-selection applied, while the last column specifies the selection defining the different signal regions.

Six signal regions are defined in order to obtain good signal sensitivity for the various models and parameter values studied. The selection applied has been chosen by optimising the expected significance in models in which pair-produced gluinos decay with 100% branching ratio to on- and off-shell scalar bottom quarks. The signal regions are characterised by the minimum number of b-jets in the final state and by different thresholds on m_{eff}, and labelled with the prefix SR0. They are summarised in the upper row of Table 2, together with a summary of the full selection applied.

For the 1-lepton channel, events are required to have exactly one lepton, a leading jet with $p_{\mathrm{T}} > 60$ GeV, three further jets with $p_{\mathrm{T}} > 50$ GeV, and $E_{\mathrm{T}}^{\mathrm{miss}} > 80$ GeV. At least one jet is required to be b-tagged. SM background processes that lead to the production of a W boson in the final state are rejected by a further selection applied on $m_{\mathrm{T}} > 100$ GeV. Two signal regions, labelled with the prefix SR1 and summarised in Table 2, are defined, based on different thresholds

applied on the effective mass and the missing transverse momentum.

6 Background Estimation

Pre-selection	Control region name	Selection
one lepton, three jets $p_{\mathrm{T}}(j1) > 130$ GeV, $p_{\mathrm{T}}(j2,j3) > 50$ GeV, $E_{\mathrm{T}}^{\mathrm{miss}} > 130$ GeV, 40 GeV $< m_{\mathrm{T}} <$ 100 GeV, $m_{\mathrm{eff}} > 600$ GeV	CR0-1 CR0-2	one b-tag two b-tag
one lepton, four jets $p_{\mathrm{T}}(j1) > 60$ GeV, $p_{\mathrm{T}}(j2,j3,j4) > 50$ GeV, $E_{\mathrm{T}}^{\mathrm{miss}} > 80$ GeV, 40 GeV $< m_{\mathrm{T}} <$ 100 GeV, $m_{\mathrm{eff}} > 500$ GeV	CR1	one b-tag

Table 3: Control regions definition for the 0-lepton and 1-lepton channels. The first column summarises the common pre-selection applied, while the last column specifies the selection defining the control regions.

Standard Model processes contributing to the total background in the signal regions are top quark production (single and in pairs), the production of a W or a Z boson in association with heavy-flavour quarks (mostly b, but also c), and multi-jet production. The latter enters in the signal regions if missing transverse momentum is produced in the final state, either because of the mis-measurement of one or more of the jets in the event, or because of the semileptonic decay of a heavy-flavour hadron.

Control Region	top	W/Z	QCD/ di-boson	SM	data (2.05 fb^{-1})
CR0-1 (1 ele)	187	48	1	235 ± 45	217
CR0-1 (1 muon)	146	22	1	169 ± 45	177
CR0-2 (1 ele)	53	2	0.1	55 ± 20	64
CR0-2 (1 muon)	42	3	0.1	45 ± 17	62
CR1 (1 ele)	414	40	3.6	460 ± 100	465
CR1 (1 muon)	377	25	5.2	410 ± 110	420

Table 4: Expected background composition and comparison of the predicted total SM event yield to the measured event yield for 2.05 fb^{-1} for each of the control regions defined in the text. The column "Top" includes contributions from the single top, $t\bar{t}$, $t\bar{t}b\bar{b}$ and $t\bar{t}+W/Z$ production processes. The quoted uncertainty on the SM prediction includes only detector-level systematic uncertainties (among which jet energy scale and b-tagging uncertainties are dominant).

Top and W/Z background estimation: The dominant SM background contributions to the signal regions are evaluated using control regions with low expected yields from the targeted SUSY signals. They are defined by selecting events containing exactly one lepton, large m_{eff} and low m_{T}. The background estimation in each signal region is obtained by multiplying the number of events observed in the corresponding control region by a transfer factor, defined as the ratio of the MC predicted yield in the signal region to that in the control region:

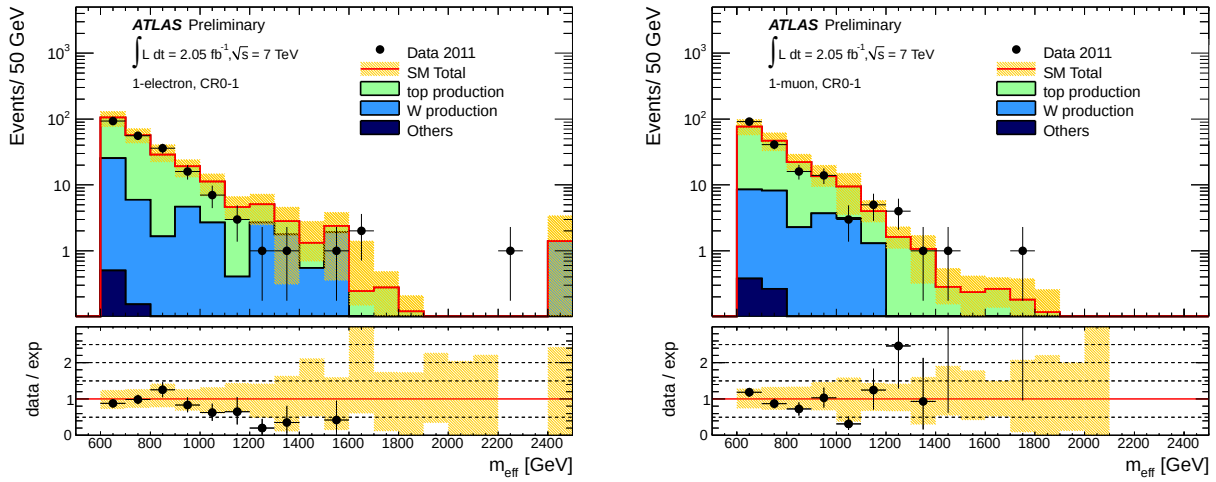

(a)

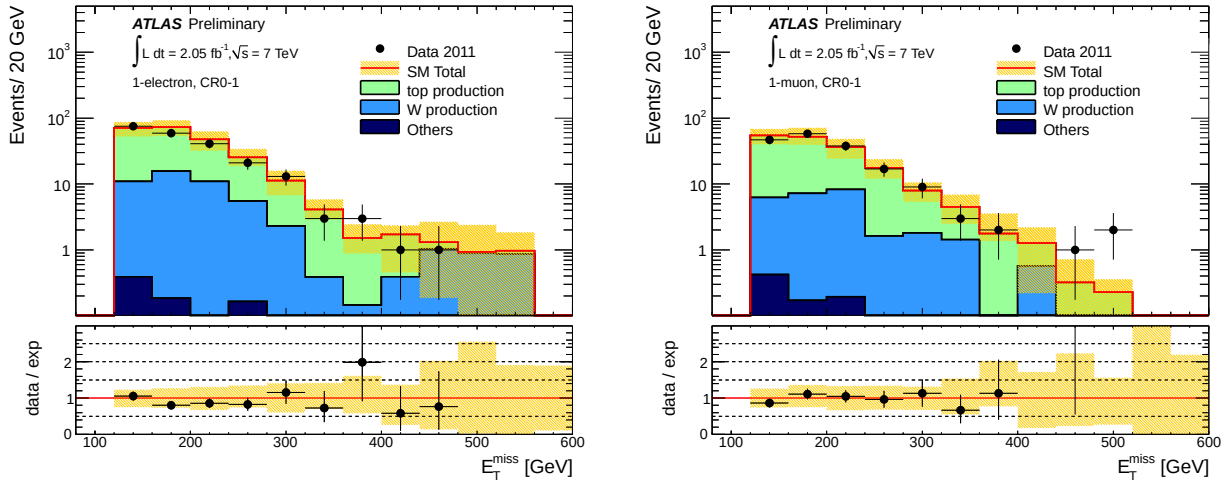

(b)

Figure 1: Distribution of (a) the effective mass and (b) $E_{\mathrm{T}}^{\mathrm{miss}}$ in the CR0-1 control region for the 1-electron (left) and 1-muon (right) channels. The color labelled "Others" includes contributions from Z, di-boson and multi-jet production processes. The yellow band shows the systematic uncertainty, which includes both detector uncertainties (among which JES and b-tagging uncertainties are dominant) and theory uncertainties on the background normalisation and shape. The small inset shows the ratio between the observed distribution and that predicted for the Standard Model background. Although the distributions are presented separately for e and μ, the background estimation uses the sum of the e and μ yields in the CR0.

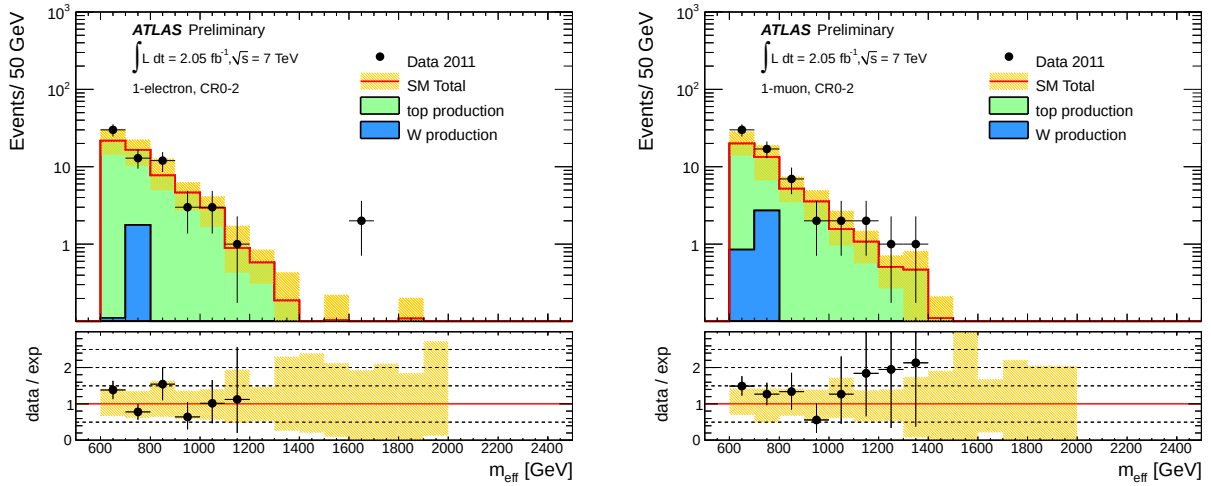

(a)

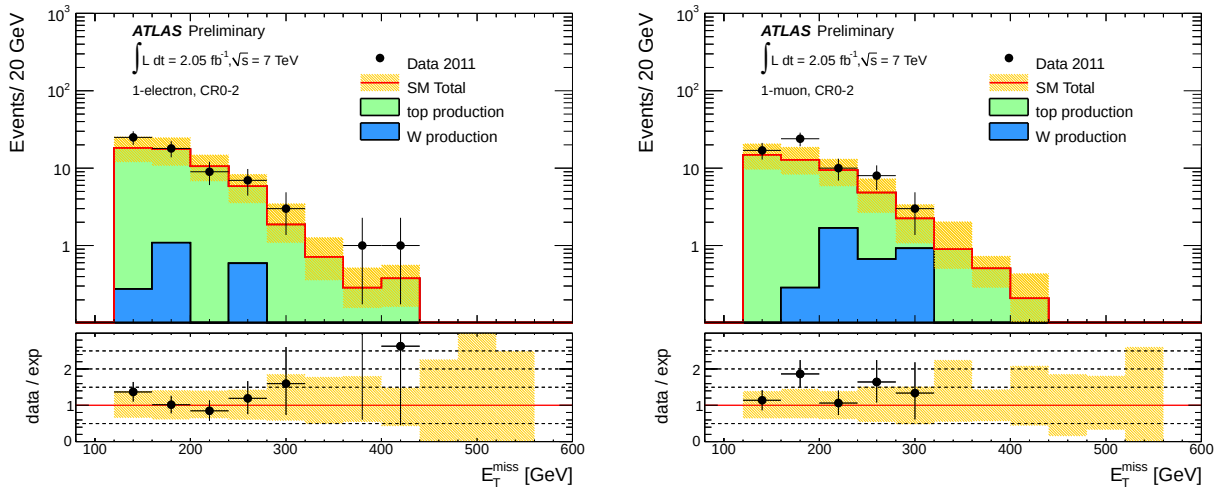

(b)

Figure 2: Distribution of (a) the effective mass and (b) $E_{\mathrm{T}}^{\mathrm{miss}}$ in the CR0-2 control region for the 1-electron (left) and 1-muon (right) channels. The yellow band shows the systematic uncertainty, which includes both detector uncertainties (among which JES and *b*-tagging uncertainties are dominant) and theory uncertainties on the background normalisation and shape. The small inset shows the ratio between the observed distribution and that predicted for the Standard Model background. Although the distributions are presented separately for e and μ, the background estimation uses the sum of the e and μ yields in the CR0.

$$N_{\rm SR} = \frac{N_{\rm SR}^{\rm MC}}{N_{\rm CR}^{\rm MC}} N_{\rm CR}^{\rm obs} = T_f N_{\rm CR}^{\rm obs} \tag{4}$$

where $N_{\rm CR}^{\rm obs}$ denotes the observed yield in the control region for single and pair produced top quarks (for SR0) or for the full SM background (for SR1). The advantage of this approach is that systematic uncertainties that are correlated between the numerator and the denominator of T_f largely cancel out, provided that the event kinematics in the corresponding signal and control region are similar.

Two control regions, differing only by the number of minimum b-tags required, are used to determine the top background in the six signal regions of the 0-lepton channel. They are obtained by applying the same thresholds on the three jets and $E_{\rm T}^{\rm miss}$ as for the SR0, but requiring exactly one signal electron or muon. The definition of the CR0-1 and CR0-2 is completed by additional selections on the transverse mass, 40 GeV$< m_{\rm T} <$ 100 GeV, on the effective mass $m_{\rm eff} >$ 600 GeV and by the requirement of at least one b-tag or two b-tags respectively. The definition of the control regions for the 0-lepton channel is summarised in the upper part of Table 3. Figures 1 and 2 shows the $E_{\rm T}^{\rm miss}$ and $m_{\rm eff}$ distributions obtained in CR0-1 and CR0-2 respectively, for the 1-electron and 1-muon case.

The formula used to obtain the top background prediction in each of the six signal regions is:

$$N_{\text{SR0-}\alpha j} = T_f^{\alpha j}(N_{\text{CR0-}j} - M_{\text{CR0-}j}^{\text{non-top}}) \tag{5}$$

$$T_f^{\alpha j} = \frac{M_{\text{SR0-}\alpha j}}{M_{\text{CR0-}j}} \tag{6}$$

where $\alpha = A, B, C$, $j = 1, 2$ denote the six signal regions, the symbol N (M) is used for observed (MC predicted quantities) and CR0-j is the sum of the corresponding electron and muon channel yields.

The rest of the SM production contributions to the SR0 is mainly due to W and Z production in association with heavy-flavour quarks. It corresponds to about 30% (10%) of the total background in the signal regions defined with one b-tag (two b-tags), and it is estimated using the MC simulation.

For the 1-lepton channel signal regions, the total SM background (largely dominated by top quark production) is determined using a similar technique, but using one single transfer factor for top, W/Z and di-boson production processes. In this case, only one control region (CR1) is defined by requiring the same kinematical cuts applied in SR1-D, with the exception of those on $m_{\rm T}$ (which is inverted) and on $m_{\rm eff}$ (whose threshold is lowered to 500 GeV). The last row of Table 3 summarises the event selection for the 1-lepton control region. Figure 3 shows the $E_{\rm T}^{\rm miss}$ and $m_{\rm eff}$ distributions in CR1.

The number of expected events for 2.05 fb^{-1} of integrated luminosity as predicted by the MC for all control regions is compared to that obtained in data in Table 4. The uncertainty quoted on the Standard Model prediction includes experimental systematic uncertainties (jet energy scale and resolution, b-tagging efficiency, lepton identification and energy scale, and luminosity determination).

Further selection regions are used to validate the MC prediction in different kinematic regimes (in particular for small and large values of $m_{\rm T}$ at low value of $m_{\rm eff}$, for both the 0-lepton and 1-lepton channels). In all cases, a good agreement between the data and MC predictions is found.

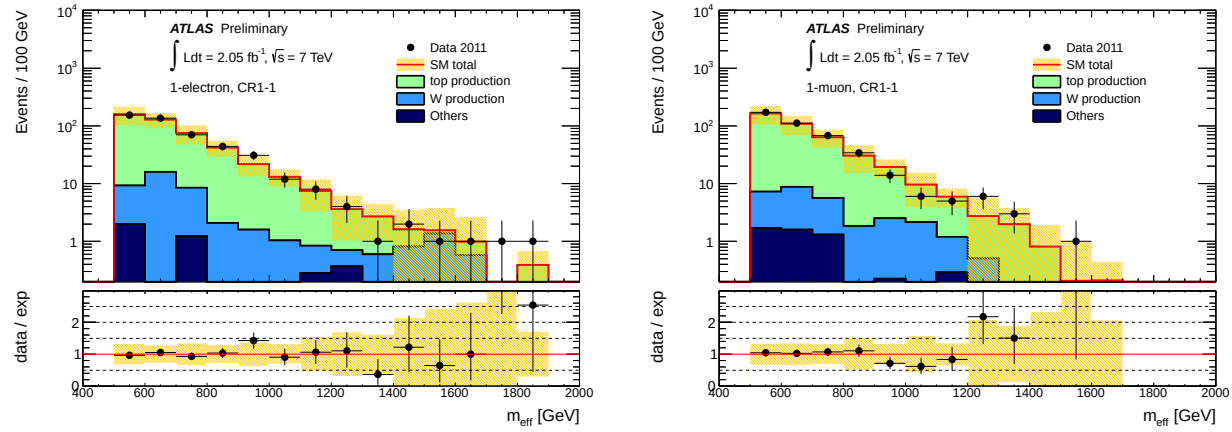

(a)

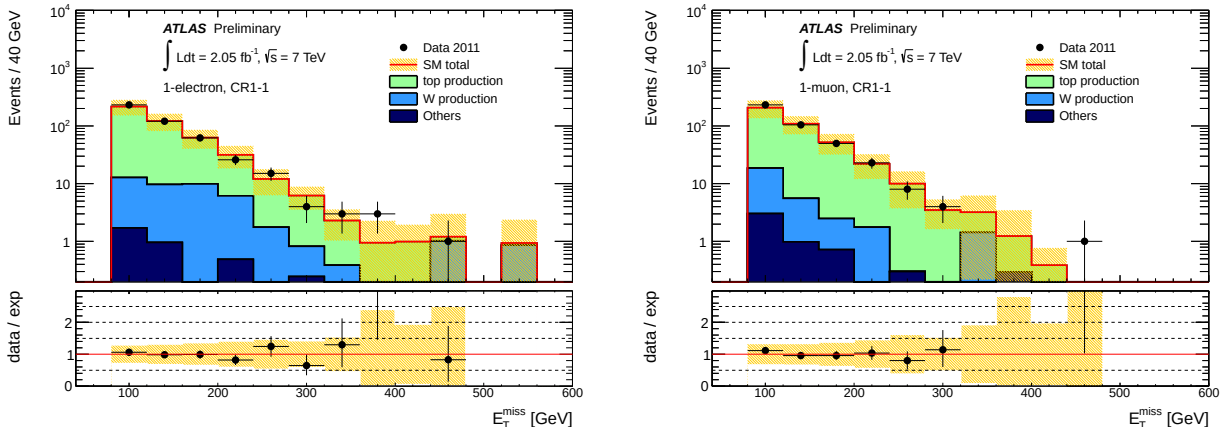

(b)

Figure 3: Distribution of (a) the effective mass and (b) $E_{\mathrm{T}}^{\mathrm{miss}}$ in the CR1 control region for the 1-electron (left) and 1-muon (right) channel. The color labelled "Others" includes contributions from Z, di-boson and multi-jet production processes. The yellow band shows the systematic uncertainty, which includes both detector uncertainties (among which JES and b-tagging uncertainties are dominant) and theory uncertainties on the background normalisation and shape. The small inset shows the ratio between the observed distribution and that predicted for the Standard Model background.

Multi-jet background estimation: The contribution of multi-jet background in the SR0 signal region is estimated with the use of a jet response smearing technique [51]. Multi-jet events with possibly large $E_{\mathrm{T}}^{\mathrm{miss}}$ are obtained by smearing jet energies in low $E_{\mathrm{T}}^{\mathrm{miss}}$ "seed" events according to jet response functions obtained with the MC simulation. The Gaussian core of the response function is tuned to data by considering the jet balance in di-jet events, while its non-Gaussian tail is adapted to reproduce the response in three-jet events where the $E_{\mathrm{T}}^{\mathrm{miss}}$ can be unambiguously associated to a single jet.

The number of multi-jet events in the SR1 signal region is estimated using a matrix method similar to the one described in Ref. [52]. The probability of misidentifying a tight lepton is estimated by computing the probability that pre-selected leptons are identified as signal leptons in low-$E_{\mathrm{T}}^{\mathrm{miss}}$ control regions dominated by multi-jet events.

7 Systematic uncertainties on background estimation

Various systematic uncertainties affecting the background rates in the signal regions have been considered. Detector-level systematic uncertainties arise from several sources:

Jet energy scale and resolution uncertainty: The uncertainty on the jet energy scale (JES), derived using single particle response and test beam data, varies as a function of the jet p_{T} and pseudorapidity and it is about 2% at $p_{\mathrm{T}} = 50$ GeV in the central detector region. Additional systematic uncertainties arise from the dependence of the jet response on the number of expected interactions per bunch crossing and on the jet flavour. The total jet energy scale uncertainty at $p_{\mathrm{T}} = 50$ GeV in the central detector region is about 5% [45]. The jet energy scale uncertainty is propagated to obtain an uncertainty on the event yield by varying it by $\pm 1\sigma$ in the MC simulation. Uncertainties related to the jet energy resolution (JER) are obtained with an in-situ measurement of the jet response asymmetry in di-jet events [53]. Their impact on the event yield is estimated by applying an additional smearing to the jet transverse momenta. The JES and JER uncertainties on the event yield amount to a total of 20-40% (depending on the signal region) and are completely dominated by the JES uncertainty.

***b*-tagging efficiency and mis-tagging uncertainties:** The uncertainty associated to the tagging procedure used to identify *b*-jets is evaluated by varying the *b*-tagging efficiency and mis-tagging rates within the error of the values measured in-situ [46]. The resulting uncertainty on the event yield is about 20% (35%) in the one *b*-tag (two *b*-tags) signal region.

Further detector-level uncertainties: Other systematic uncertainties arise from the imperfect knowledge of the lepton identification efficiency and energy scale, the rate of lepton misidentification and from the luminosity determination. Their contribution to the final uncertainty is found to be negligibly small.

All the detector-level systematic uncertainties are included, together with process-specific uncertainties, in the evaluation of the background uncertainty:

Multi-jet background: The systematic uncertainty on the estimation of the multi-jet background in the SR0 is determined by taking into account statistical uncertainties and possible biases in the selection of the seed events, as well as uncertainties in the tuning of the tail of the

jet response function in the three-jet events. The total uncertainty varies between 50% and 70% depending on the SR0 considered.

The estimated multi-jet background in the SR1 is affected by systematic uncertainties related to the determination of the lepton misidentification rate and to the subtraction of non-multi-jet contributions to the event yield in the multi-jet enhanced region. The estimated uncertainty is 90% and 100% in SR1-D and SR1-E respectively.

***W* and *Z* production processes:** Systematic uncertainties on W and Z production are evaluated by using ALPGEN MC predictions. Event generation uncertainties are evaluated by varying the relative cross section of the samples generated with different numbers of outgoing partons [54], resulting in an uncertainty of about 30%. Additional uncertainties of about 70% on the production cross section of W and Z bosons in association with b-quarks are considered. They are derived from direct measurements [16,55], and extrapolated using the MC simulation to include differences in the phase space regions probed by this analysis.

SR	JES/ JER	b-tag	lepton ID	top theory	others	total
SR0-A1	4	3	2	11	10	15
SR0-B1	3	3	2	20	10	22
SR0-C1	3	4	2	35	11	37
SR0-A2	3	3	2	15	17	23
SR0-B2	3	4	2	20	10	22
SR0-C2	3	2	2	30	12	32
SR1-D	6	1	1	34	7	35
SR1-E	7	1	1	53	10	55

Table 5: Relative systematic uncertainties (in percent) associated to the background estimated by using transfer factors for all the signal regions considered. The column "others" includes statistical uncertainties on the event yield in the control regions, and, in the case of the 0-lepton channel, systematic uncertainties on the non-top production contributions subtracted from the control regions. The column "top theory" contains residual theoretical uncertainties on the top production process addressed as discussed in the text.

Top production processes: Theoretical uncertainties on the shape of $t\bar{t}$ and single top kinematical distributions are evaluated by comparing different LO and NLO generators (ALPGEN or POWHEG, the latter using both PYTHIA and HERWIG as parton shower), and using different parton shower tunes, still consistent with data from previous experiments [54].

The T_f, used for the top and total SM background determination in the SR0 and SR1 respectively, are computed using MC predictions. Their values span from 1.8 to 0.05 depending on the signal region considered. Their associated uncertainty arises from both detector-level (JES and JER, b-tagging efficiency and fake rate, lepton identification and energy scale) and event generator level uncertainties. The use of control regions with similar kinematical properties to those of the signal regions strongly suppresses detector-level uncertainties. Theoretical uncertainties typically dominate the total uncertainty on the T_f, which varies between 15% and 35%.

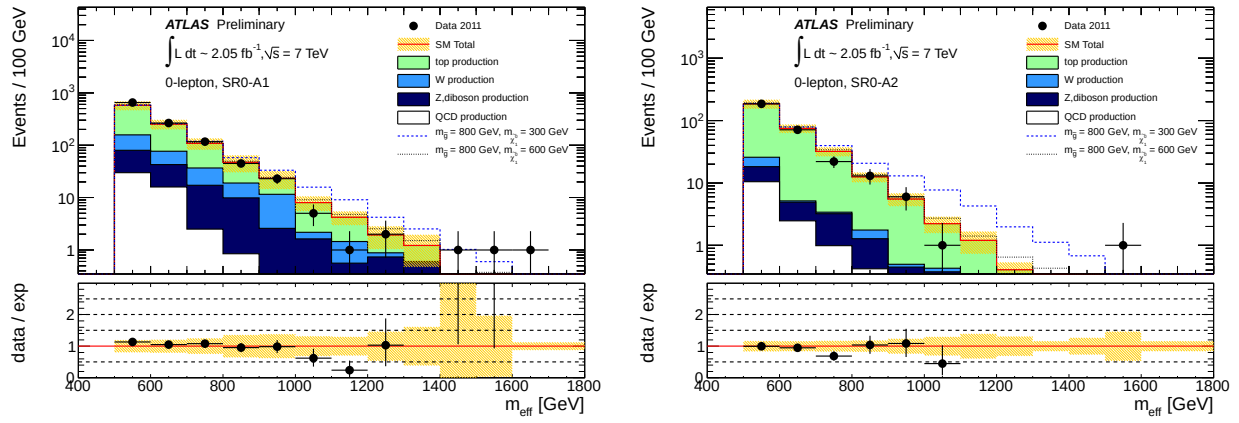

(a)

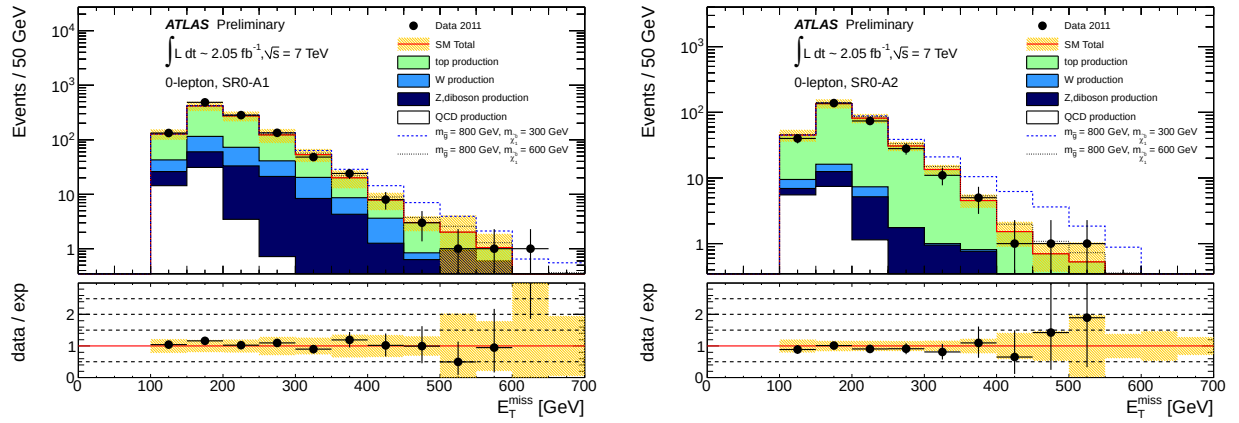

(b)

Figure 4: Distribution of (a) the effective mass and (b) $E_{\mathrm{T}}^{\mathrm{miss}}$ in SR0-A1 (left) and SR0-A2 (right). The yellow band shows the systematic uncertainty, which includes both detector uncertainties (among which JES and b-tagging uncertainties are dominant) and theory uncertainties on the background normalisation and shape. The small inset shows the ratio between the observed distribution and that predicted for the Standard Model background.

A summary of the systematic uncertainties for the background estimates with the use of transfer factors is shown in Table 5.

8 Results

The m_{eff} and $E_{\mathrm{T}}^{\mathrm{miss}}$ distributions are shown in Figure 4 for SR0-A1 and SR0-A2, and in Figure 5 for SR1-D. Tables 6 and 7 show the Standard Model background predictions and the observed number of events corresponding to 2.05 fb^{-1} in all signal regions. The top background uncertainty in the 0-lepton (1-lepton) signal regions corresponds to the total systematic uncertainty of Table 5. The W/Z background in the SR0 corresponds to the MC prediction. The multi-jet background contribution in the SR0 is summed together with that of di-boson background.

The results are consistent with the Standard Model predictions, and they are therefore translated into 95% confidence-level (C.L.) upper limits on contributions from new physics using the CL$_{\mathrm{s}}$ prescription [56]. The likelihood function used is written as $L(n|s,b,\theta) = P_{\mathrm{s}} \times C_{\mathrm{Syst}}$; where

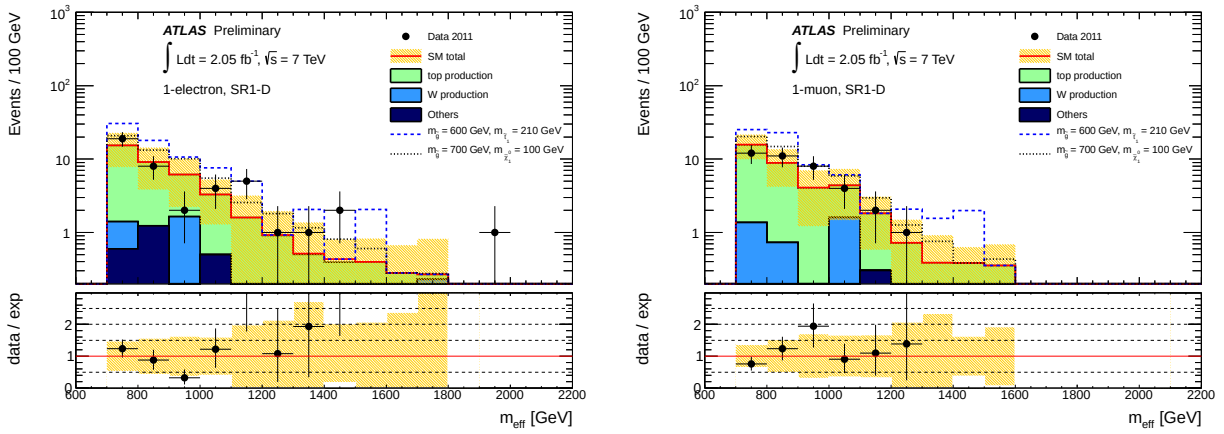

(a)

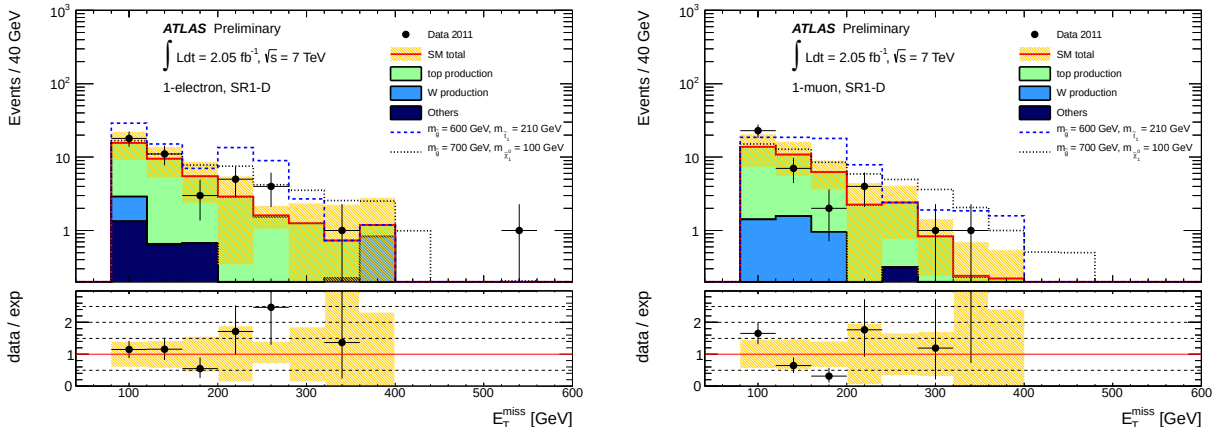

(b)

Figure 5: Distribution of (a) the effective mass and (b) $E_{\mathrm{T}}^{\mathrm{miss}}$ for the 1-electron (left) and 1-muon (right) channel in SR1-D. The color labelled "Others" includes contributions from Z, di-boson and multi-jet production processes. The yellow band shows the systematic uncertainty, which includes both detector uncertainties (among which JES and b-tagging uncertainties are dominant) and theory uncertainties on the background normalisation and shape. The small inset shows the ratio between the observed distribution and that predicted for the Standard Model background.

SR	Top	W/Z	QCD/ di-boson	Total	Data
SR0-A1	705 ± 110 (725)	248 ± 150	53 ± 21	1000 ± 180	1112
SR0-B1	119 ± 26 (122)	67 ± 42	7.3 ± 4.7	190 ± 50	197
SR0-C1	22 ± 9 (22)	16 ± 11	1.5 ± 1	39 ± 14	34
SR0-A2	272 ± 70 (212)	22.5 ± 15	21 ± 12	316 ± 72	299
SR0-B2	47 ± 11 (37)	4.5 ± 3	2.8 ± 1.7	54 ± 11	43
SR0-C2	8.5 ± 3 (6.6)	0.8 ± 1	0.5 ± 0.4	9.8 ± 3.2	8

Table 6: Summary of the expected and observed event yields corresponding to 2.05 fb^{-1} in the six 0-lepton channel signal regions. The errors on the top contribution correspond to the total errors of Table 5. The errors quoted for all background processes include all the systematic uncertainties discussed in the text. The numbers in parentheses in the "Top" column are the yields predicted by the MC simulation.

SR	SM background	Data
SR1-D (e)	39 ± 12 (39)	43
SR1-D (μ)	38 ± 14 (37)	38
SR1-E (e)	8.1 ± 3.4 (7.9)	11
SR1-E (μ)	6.3 ± 4.2 (6.1)	6

Table 7: Summary of the expected and observed event yields corresponding to 2.05 fb^{-1} in the two 1-lepton channel signal regions. The Standard Model estimation is derived with the data-driven method discussed in the text. The numbers in parenthesis in the "SM background" column are the yield predicted by the MC.

n represents the number of observed events in data, s is the SUSY signal under consideration, b is the background, and θ represents the systematic uncertainties. The P_s function is a Poisson-probability distribution for event counts in the defined signal region and C_{Syst} represents the constraints on systematic uncertainties, which are treated as nuisance parameters with a Gaussian probability density function and correlated when appropriate.

Upper limits at 95% C.L. on the number of signal events in the signal regions are obtained independently of new physics models for the 0-lepton and 1-lepton final states. Results for observed and expected upper limits on the number of non-Standard Model events in the signal regions are shown in Table 8, as well as upper limits on the visible cross section, σ_{vis}, including the effects of experimental acceptance and efficiency.

SR	95% C.L. upper limit	
	N events	σ_{vis}(fb)
	obs. (exp.)	obs. (exp.)
SR0-A1	578 (516)	282 (251)
SR0-B1	133 (133)	65 (65)
SR0-C1	31.6 (34.6)	15.4 (16.9)
SR0-A2	124 (134)	61 (66)
SR0-B2	29.6 (31.0)	14.4 (15.0)
SR0-C2	8.9 (10.3)	4.3 (5.0)
SR1-D	45.5 (42.1)	22.2 (20.5)
SR1-E	17.5 (15.3)	8.5 (7.5)

Table 8: Observed and expected 95% C.L. upper limits on the non-SM contributions to all signal regions. Limits are given on the number of signal events and in terms of visible cross sections. The systematic uncertainties on the SM background estimation are included.

9 Interpretation in Simplified SUSY Models

The interpretation of the results in terms of 95% C.L. exclusion limits are given for several SUSY scenarios.

Simplified models are characterised by well-defined SUSY particle production and decay modes yielding the final states under study. In the scenarios considered here scalar bottoms and tops are the only squarks to appear in the gluino decay cascade, leading to final states with large b-jet multiplicity. The models listed below are addressed (in parenthesis the channel which is used for the interpretation of the result is given):

Gluino-sbottom models (0-lepton): MSSM scenarios where the $\tilde{b}_1$ is the lightest squark, all other squarks are heavier than the gluino, and $m_{\tilde{g}} > m_{\tilde{b}_1} > m_{\tilde{\chi}_1^0}$, such that the branching ratio for $\tilde{g} \to \tilde{b}_1 b$ decays is 100%. Sbottoms are produced via $\tilde{g}\tilde{g}$ and $\tilde{b}_1\tilde{b}_1$ and are assumed to decay exclusively via $\tilde{b}_1 \to b\tilde{\chi}_1^0$, where $m_{\tilde{\chi}_1^0}$ is set to 60 GeV. Exclusion limits are presented in the $(m_{\tilde{g}}, m_{\tilde{b}_1})$ plane.

Gbb models (0-lepton): Simplified scenarios, where $\tilde{b}_1$ is the lightest squark but $m_{\tilde{g}} < m_{\tilde{b}_1}$. Pair production of gluinos is the only process taken into account since the mass of all other sparticles is set above the TeV scale. A three-body decay via off-shell sbottom is assumed for gluino, such that $\tilde{b}_1{}^{(*)} \to b\tilde{\chi}_1^0$ (BR=100% for $b\bar{b}\tilde{\chi}_1^0$). Exclusion limits are presented in the $(m_{\tilde{g}}, m_{\tilde{\chi}_1^0})$ plane.

Gluino-stop models (1-lepton): MSSM scenarios where the $\tilde{t}_1$ is the lightest squark, all other squarks are heavier than the gluino, and $m_{\tilde{g}} > m_{\tilde{t}_1} + m_t$, such that the branching ratio for $\tilde{g} \to \tilde{t}_1 t$ decays is 100%. Stops are produced via $\tilde{g}\tilde{g}$ and $\tilde{t}_1\tilde{t}_1$ and are assumed to decay exclusively via $\tilde{t}_1 \to b\tilde{\chi}_1^{\pm}$. The neutralino mass is set to 60 GeV, the chargino mass to 120 GeV and the latter is assumed to decay through a virtual W boson (BR($\tilde{\chi}_1^{\pm} \to \tilde{\chi}_1^0 l^{\pm}\nu$)=11%). If $m_{\tilde{t}_1} > m_{\tilde{\chi}_1^0} + m_t$, the decay $\tilde{t}_1 \to t\tilde{\chi}_1^0$ is also kinematically allowed, with BR depending on the MSSM parameters settings. However, this mode is not considered for this interpretation, leading to conservative results, and is adopted in the *Gtt* scenario, described below. Exclusion limits are presented in the $(m_{\tilde{g}}, m_{\tilde{t}_1})$ plane.

Gtt models (1-lepton): Simplified scenarios, where $\tilde{t}_1$ is the lightest squark but $m_{\tilde{g}} < m_{\tilde{t}_1}$. Pair production of gluinos is the only process taken into account since the mass of all other sparticles is set above the TeV scale. A three-body decay via off-shell stop is assumed for the gluino, such that $\tilde{t}_1{}^{(*)} \to t\tilde{\chi}_1^0$ (BR=100% for $t\bar{t}\tilde{\chi}_1^0$). Exclusion limits are presented in the $(m_{\tilde{g}}, m_{\tilde{\chi}_1^0})$ plane.

Gtb models (1-lepton): Simplified scenarios, where $\tilde{b}_1$ and $\tilde{t}_1$ are the lightest squarks but $m_{\tilde{g}} < m_{\tilde{b}_1, \tilde{t}_1}$. As for the models above, pair production of gluinos is the only process taken into account, with gluinos decaying via virtual stops or sbottoms with a BR of 100% assumed for $\tilde{t}_1 \to b + \tilde{\chi}_1^{\pm}$ and $\tilde{b}_1 \to t + \tilde{\chi}_1^{\pm}$, respectively. The mass difference between charginos and neutralinos is set to 2 GeV, such that the products of $\tilde{\chi}_1^{\pm} \to \tilde{\chi}_1^0 + f\bar{f}'$ are invisible to the event selection, and gluino decays result in three-body final states ($b\bar{t}\tilde{\chi}_1^0$ or $t\bar{b}\tilde{\chi}_1^0$). Exclusion limits are presented in the $(m_{\tilde{g}}, m_{\tilde{\chi}_1^0})$ plane.

The zero-lepton analysis is mostly sensitive to the SUSY scenarios where sbottom production dominates, whilst the 1-lepton analysis results are employed to set exclusion limits in models characterised by on-shell or off-shell stop production, where top-enriched final states are expected. Since several signal regions are defined for each analysis, the SR with the best expected sensitivity at each point in parameter space is adopted as the nominal result across the different planes.

The efficiency times acceptance of the selection strongly depends on the parameters of the model and the signal region considered. It varies between 5% and 50% in the proximity of the expected limit for the gluino-sbottom model. For the *Gbb* models, the efficiency times acceptance is highly dependent on the difference in mass between the gluino and the neutralino. It is about 1% for a mass difference of about 200 GeV, and it increases up to 45% for larger mass splitting. In the *Gtb*, gluino-stop and *Gtt* models, the efficiency times acceptance varies typically between 1 and 20% in the proximity of the expected limit.

Systematic uncertainties on the signal include detector-related (JES, JER, *b*-tagging) and theory uncertainties. Detector-related uncertainties are considered fully correlated with those obtained for the background, and they typically amount to 10-30% depending on the signal region and model considered. Theory uncertainties on the expected SUSY signal are estimated

by varying the factorisation and renormalisation scales in PROSPINO between half and twice their default values and by considering the PDF uncertainties provided by CTEQ6. Uncertainties are calculated for individual production processes and are typically 20-35% in the vicinity of the expected limit.

Figure 6 shows the observed and expected exclusion regions in the $(m_{\tilde{g}}, m_{\tilde{b}_1})$ plane for the gluino-sbottom model. The selection SR0-C2 provides the best sensitivity in most cases. If $m_{\tilde{g}} - m_{\tilde{b}_1} < 100$ GeV, signal regions with one b-tag are preferred, due to the lower number of expected b-jets above p_{T} thresholds. Gluino masses below 920 GeV are excluded for sbottom masses up to about 800 GeV. The exclusion is less stringent in the region with low $m_{\tilde{g}} - m_{\tilde{b}_1}$, where low $E_{\mathrm{T}}^{\mathrm{miss}}$ is expected. This search extends the previous ATLAS exclusion limit in the same scenario by about 200 GeV, and it is complementary to direct searches for sbottom pair production published by the ATLAS collaboration [16] using the same data-set. The limits do not strongly depend on the neutralino mass assumption as long as $m_{\tilde{g}} - m_{\tilde{\chi}_0}$ is larger than 300 GeV, due to the harsh kinematic cuts.

The interpretation of the results in the *Gbb* models, defined in the $(m_{\tilde{g}}, m_{\tilde{\chi}_1^0})$ plane at sbottom mass larger than 1 TeV, can be considered complementary to the previous one, defined in $m_{\tilde{g}}, m_{\tilde{b}_1}$ at fixed $\tilde{\chi}_1^0$ mass. Figure 7 shows the expected and observed exclusion limit contours and the maximum 95% upper cross section limit for each model. Gluino masses below 900 GeV are excluded for neutralino masses up to about 300 GeV.

Figures 8 to 10 report the interpretations of the 1-lepton analysis results in different scenarios. As for the 0-lepton results, the selection yielding the best expected limit for a given parameter point is used. The observed and expected exclusion limit contours at 95% C.L. are estimated taking into account possible signal contamination in the control regions employed to measure the SM background contributions.

Figure 8 shows upper limits in the $(m_{\tilde{g}}, m_{\tilde{t}_1})$ plane for the gluino-stop model. Gluino masses below 620 GeV are excluded at 95% C.L. for stop masses up to 440 GeV. The observed and expected upper limits at 95% C.L. extracted in the $(m_{\tilde{g}}, m_{\tilde{\chi}_1^0})$ plane for the *Gtt* models are shown in Figure 9. The upper cross section limits at 95% C.L. are also reported for each MSSM scenario. In this case, gluino masses below 750 GeV are excluded at 95% C.L. for $m_{\tilde{\chi}_1^0} = 50$ GeV while neutralino masses below 160 GeV are excluded at 95% C.L. for $m_{\tilde{g}} = 700$ GeV.

Figure 10 shows upper limits at 95% C.L. for the *Gtb* models. Only scenarios with chargino masses above the experimental limits from LEP experiments are considered, and gluino masses below 720 GeV are excluded at 95% C.L. for $m_{\tilde{\chi}_1^0} = 100$ GeV while neutralino masses below 200 GeV are excluded at 95% C.L. for $m_{\tilde{g}} = 600$ GeV. The contribution of the 0-lepton channel signal regions to the significance has been also evaluated for this scenario and found to be lower than that of the 1-lepton channel.

10 Interpretation in SO(10) Models

In addition to the simplified model interpretation, results are interpreted in the context of two specific SO(10) models [60], the D-term splitting model, DR3, and the Higgs splitting model, HS. For both models the SUSY particle mass spectrum is characterised by the low masses of the gluinos (300-600 GeV), charginos (100-180 GeV) and neutralinos (50-90 GeV), whereas all scalar particles have masses beyond the TeV scale. Depending on the sparticles masses, chargino-neutralino or gluino-pair production dominates. At low gluino masses, the three-body gluino decays $\tilde{g} \to b\bar{b}\tilde{\chi}_1^0$ and $\tilde{g} \to b\bar{b}\tilde{\chi}_2^0$ dominate in the DR3 and the HS model, respectively. Final states with high b-jet multiplicities are then expected in both models with a harder $E_{\mathrm{T}}^{\mathrm{miss}}$ spectrum in

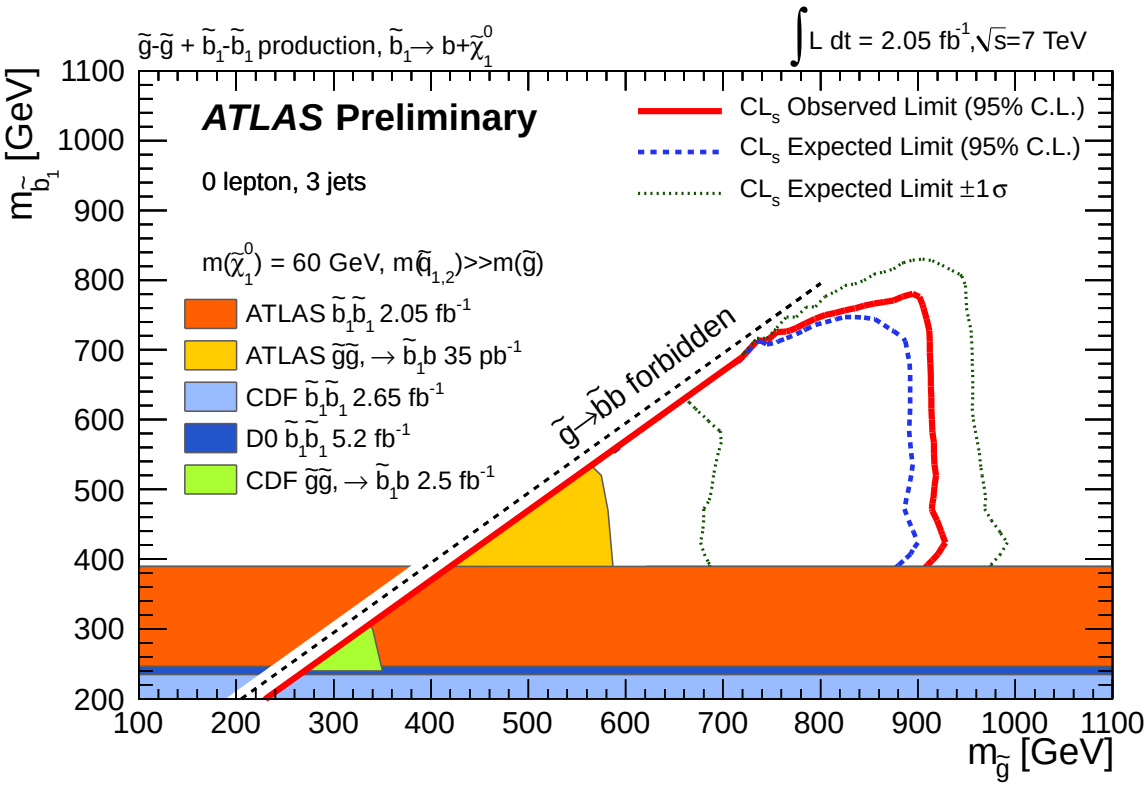

Figure 6: Observed and expected 95% C.L. exclusion limits in the $(m_{\tilde{g}}, m_{\tilde{b}_1})$ plane (gluino-sbottom models). For each scenario, the signal region providing the best expected limit is chosen. The neutralino mass is assumed to be 60 GeV and the NLO cross sections are calculated using `PROSPINO`. The result is compared to previous results from ATLAS [14] and CDF [57] searches which assume the same gluino-sbottom decays hypotheses. Exclusion limits from the CDF [58], D0 [59] and ATLAS [16] experiments on direct sbottom pair production are also shown.

the DR3 scenario due to the direct gluino decay into χ_1^0 and with a higher lepton content in the HS scenario due to the subsequent decay $\tilde{\chi}_2^0 \rightarrow \ell\bar{\ell}\tilde{\chi}_1^0$. For heavy gluinos, the gluino decay modes $\tilde{g} \rightarrow bt\tilde{\chi}_1^{\pm}$ and $\tilde{g} \rightarrow t\bar{t}\tilde{\chi}_1^0$ become more relevant, enhancing final states with leptons in both scenarios.

Results of both 0-lepton and 1-lepton analyses have been employed to extract exclusion limits at 95% C.L. on the gluino mass in the two SO(10) scenarios, DR3 and HS. The 0-lepton analysis has the best sensitivity at low gluino masses while the lepton-based selection is more sensitive to heavy gluinos. For each gluino mass, the signal region leading to the best expected significance is used to extract the 95% C.L. exclusion limits. Figure 11 shows the `PROSPINO` NLO cross-section and the observed and expected upper limit at 95% C.L. for the DR3 (Figure 11(a)) and HS (Figure 11(b)) models as a function of the gluino mass. At the nominal NLO cross section, gluino masses below 650 GeV and 620 GeV are excluded at 95% C.L. for the DR3 and HS models respectively.

These limits on the gluino masses can be interpreted in terms of Yukawa coupling unification in the third generation which is quantified as :

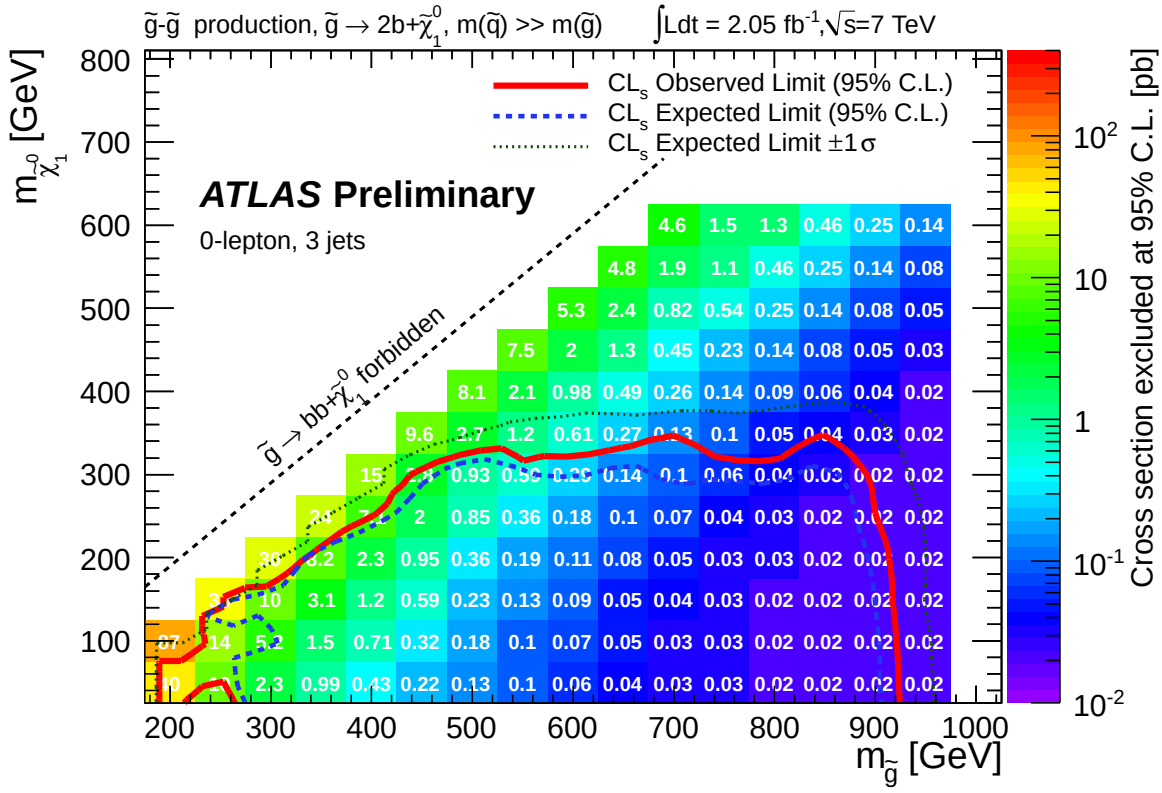

Figure 7: Observed and expected 95% C.L. exclusion limits in the $(m_{\tilde{g}}, m_{\tilde{\chi}_1^0})$ plane (*Gbb* models). For each scenario, the signal region selection providing the best expected limit is chosen.

$$R = \max(f_t, f_b, f_\tau)/\min(f_t, f_b, f_\tau) \tag{7}$$

where f_t, f_b, f_τ are the t, b and τ Yukawa couplings evaluated at the scale $Q = M_{\rm GUT}$. In both DR3 and HS model lines, the Yukawa couplings unification occurs at a few percent level for low gluino masses, while as $m_{\tilde{g}}$ increases, the Yukawa couplings unification also increases until $m_{\tilde{g}} = 650(620)$ GeV where $R = 1.14(1.1)$ for the DR3 (HS) model line. Consequently, the most favored range of gluino masses is excluded for the two SO10 model lines considered. However, Yukawa unification can still be realized at a few percent level for heavier gluino masses in different model lines [61].

11 Conclusions

An updated search for supersymmetry in final states with missing transverse momentum and at least one or two b-jets in proton-proton collisions at 7 TeV is presented. The results are based on data corresponding to an integrated luminosity of 2.05 fb^{-1} collected during 2011. The search is sensitive mainly to gluino-mediated production of sbottoms and stops, the supersymmetric partners of the third generation quarks, which, due to mixing effects, might be the lightest squarks. Since no excess above the expectations from Standard Model processes was found, the results are used to exclude parameter regions in various R-parity conserving SUSY models.

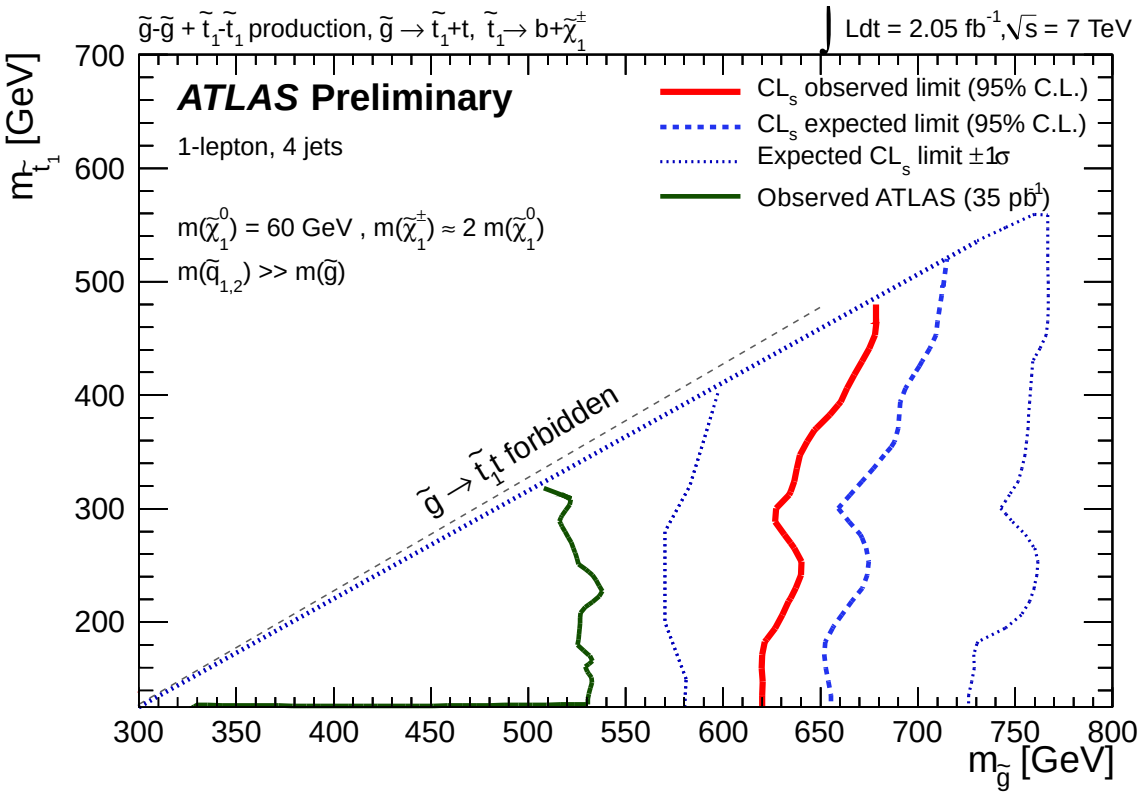

Figure 8: The observed and expected 95% C.L. exclusion limits in the $(m_{\tilde{g}}, m_{\tilde{t}_1})$ plane (gluino-stop models) using the best expected limit between SR1-D and SR1-E for each signal point. The result is compared to previous results from ATLAS [14] searches which assume the same gluino-stop decays hypotheses.

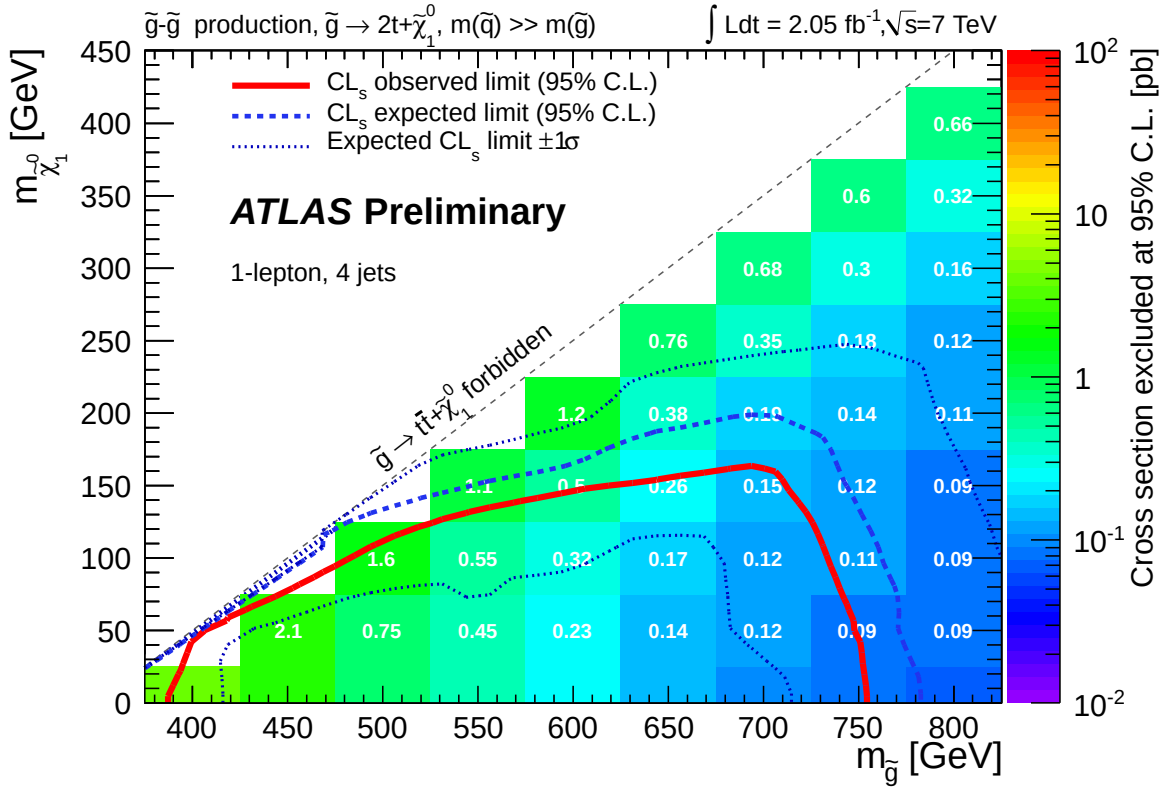

Figure 9: The observed and expected 95% C.L. exclusion limits in the $(m_{\tilde{g}}, m_{\tilde{\chi}_1^0})$ plane (*Gtt*) using the best expected limit between SR1-D and SR1-E for each signal point.

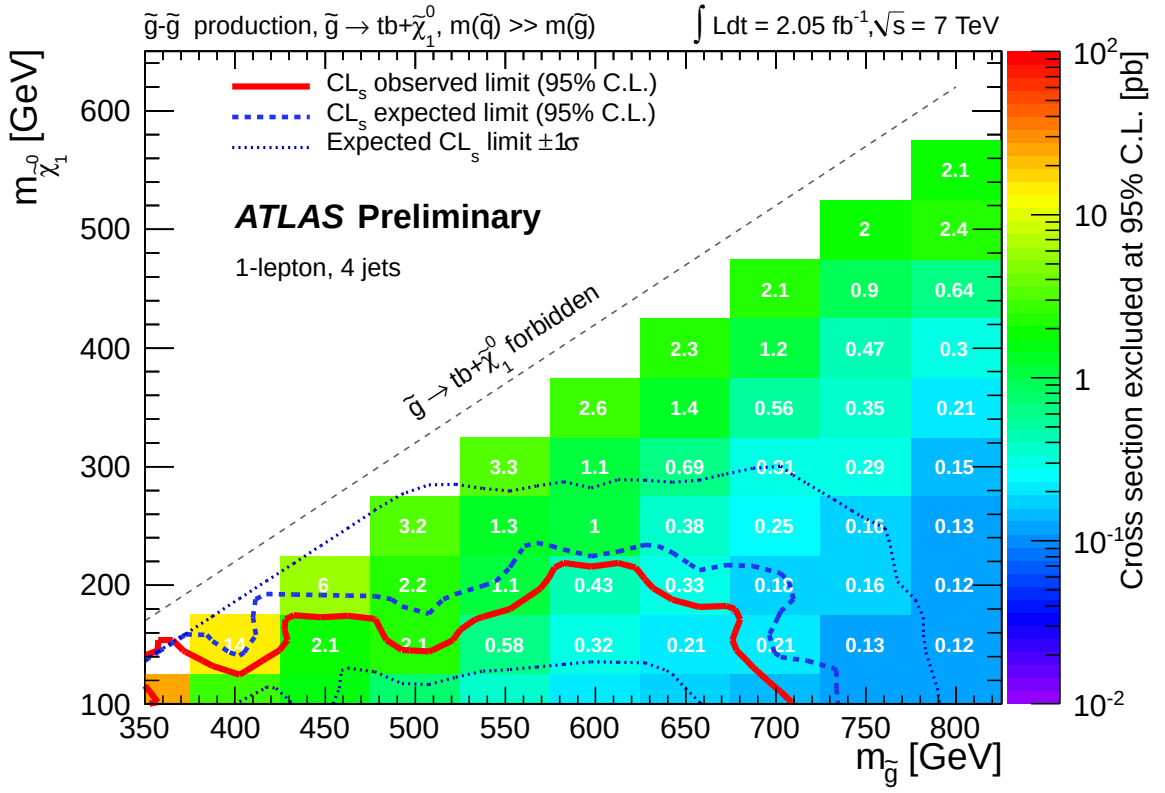

Figure 10: The observed and expected 95% C.L. exclusion limits in the $(m_{\tilde{g}}, m_{\tilde{\chi}_1^0})$ plane (*Gtb* models) using the best expected limit between SR1-D and SR1-E for each signal point.

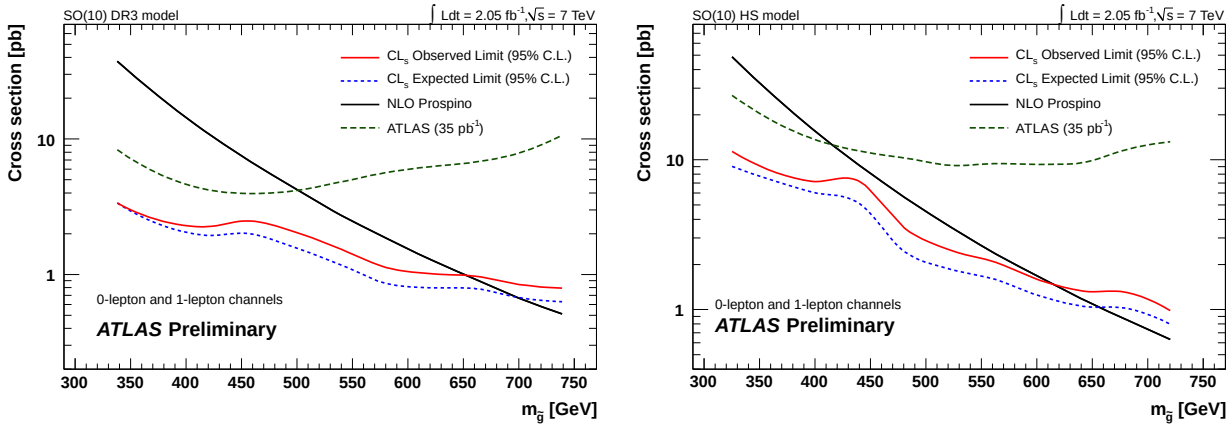

(a) (b)

Figure 11: Cross-sections as a function of the gluino mass for DR3 (a) and HS (b) models. The observed and expected 95% C.L. exclusion limits are shown respectively in red and in blue. For each gluino mass, the signal region yielding the best expected limit is used. The background estimation takes into account possible signal contamination. The NLO theoretical cross-section from PROSPINO is shown in black. The previous limit obtained with the ATLAS [14] searches in the 0-lepton plus 3 jets channel with $\mathscr{L} = 35$ pb^{-1} is superimposed for reference.

Gluino masses up to 800-900 GeV are excluded at 95% C.L. in simplified models where the squark $\tilde{b}_1$ is produced either on- or off-shell and decays in 100% of the cases into $b\tilde{\chi}_1^0$. In scenarios where the squark $\tilde{t}_1$ is produced (on- or off-shell) via gluino decay, gluino masses up to 620-750 GeV (depending on the specific model considered) are excluded at 95% C.L. In models where gluinos decay via an off-shell stop or sbottom ($bt\tilde{\chi}_1^0$ final states), gluino masses are excluded up to about 720 GeV for a neutralino mass of 100 GeV.

In specific models based on the gauge group SO(10), gluinos with masses below 650 GeV and 620 GeV are excluded for the DR3 and HS models, respectively. This analysis significantly improves the previous published limits on the same subject by the ATLAS and CMS collaborations.

References

[1] Y. Golfand and E. Likhtman, JETP Lett. **13** (1971) 323–326.

[2] A. Neveu and J. H. Schwarz, Nucl. Phys. **B31** (1971) 86–112.

[3] A. Neveu and J. H. Schwarz, Phys. Rev. **D4** (1971) 1109–1111.

[4] P. Ramond, Phys. Rev. **D3** (1971) 2415–2418.

[5] D. Volkov and V. Akulov, Phys. Lett. **B46** (1973) 109–110.

[6] J. Wess and B. Zumino, Phys. Lett. **B49** (1974) 52.

[7] J. Wess and B. Zumino, Nucl. Phys. **B70** (1974) 39–50.

[8] G. R. Farrar and P. Fayet, Phys. Lett. **B76** (1978) 575–579.

[9] P. Fayet, Phys. Lett. **B69** (1977) 489.

[10] E. Gildener and S. Weinberg, Phys. Rev. **D13** (1976) 3333.

[11] S. Weinberg, Phys. Lett. **B82** (1979) 387.

[12] H. Fritzsch and P. Minkowski, Annals of Physics **93** (1975) 193.

[13] M. Gell-Mann, P. Ramond, and R. Slansky, Rev.Mod.Phys. **50** (1978) 721.

[14] ATLAS Collaboration, Phys. Lett. **B701** (2011) 398–416.

[15] CMS Collaboration, JHEP **08** (2011) 155.

[16] ATLAS Collaboration, `arXiv:1112.3832v1 [hep-ex] (2011)`.

[17] ATLAS Collaboration, JINST **3** (2008) S08003.

[18] S. Frixione and B. Webber, hep-ph/0601192 (2006) .

[19] P. M. Nadolsky et al., Phys. Rev. **D78** (2008) 013004.

[20] S. Frixione et al., JHEP **11** (2007) 070.

[21] B. Kersevan and E. Richter-Was, hep-ph/0405247 (2004).

[22] M. Mangano et al., JHEP **07** (2003) 001.

[23] J. Pumplin et al., JHEP **07** (2002) 012.

[24] G. Corcella et al., JHEP **01** (2001) 010.

[25] J. Butterworth, J. R. Forshaw, and M. Seymour, Z. Phys. **C72** (1996) 637–646.

[26] J. Alwall, M. Herquet, F. Maltoni, O. Mattelaer, and T. Stelzer, JHEP **06** (2011) 128.

[27] T. Sjöstrand, S. Mrenna, and P. Skands, JHEP **0605** (2006) 026.

[28] M. Bahr et al., Eur. Phys. J. **C58** (2008) 639–707.

[29] W. Beenakker, M. Kramer, T. Plehn, M. Spira, and P. Zerwas, Nucl. Phys. **B515** (1998) 3–14.

[30] D. Stump et al., JHEP **10** (2003) 046.

[31] ATLAS Collaboration, ATL-PHYS-PUB-2010-014 (2010) and ATLAS-CONF-2010-031 (2010).

[32] ATLAS Collaboration, Eur. Phys. J. **C70** (2010) 823–874.

[33] GEANT4 Collaboration, S. Agostinelli et al., Nucl. Instrum. Meth. **A506** (2003) 250–303.

[34] J. Campbell and R. Ellis, Phys. Rev. D **60(113006)** (1999) .

[35] J. M. Campbell, R. K. Ellis, and C. Williams, JHEP **07** (2011) 018.

[36] R. Hamberg, W. L. van Neerven, and T. Matsuura, Nucl. Phys. **B359** (1991) 343–405. Erratum-ibid. **B644**:403-404,2002.

[37] K. Melnikov and F. Petriello, Phys. Rev. **D74** (2006) 114017.

[38] K. Melnikov and F. Petriello, Phys. Rev. Lett. **96** (2006) 231803.

[39] R. Bonciani, S. Catani, M. L. Mangano, and P. Nason, Nucl. Phys. **B529** (1998) 424–450.

[40] S. Moch and P. Uwer, Phys. Rev. **D78** (2008) 034003.

[41] M. Beneke, M. Czakon, P. Falgari, A. Mitov, and C. Schwinn, Phys. Lett. **B690** (2010) 483–490.

[42] ATLAS Collaboration, `arXiv:1110.3174 [hep-ex] (2011)`.

[43] M. Cacciari, G. Salam, and G. Soyez, JHEP **04** (2008) 063.

[44] M. Cacciari and G. Salam, Phys. Lett. B **641** (2006) no. 1, 57 – 61.

[45] ATLAS Collaboration, `arXiv:1112.6426 [hep-ex] (2011)`.

[46] ATLAS Collaboration, ATLAS-CONF-2011-102 (2011).

[47] ATLAS Collaboration, Eur. Phys. J. **C72** (2012) 1844.

[48] ATLAS Collaboration, Eur. Phys. J. **C71** (2011) 1630.

[49] ATLAS Collaboration, ATLAS-CONF-2011-116 (2011).

[50] ATLAS Collaboration, ATLAS-CONF-2012-004 (2012).

[51] ATLAS Collaboration, `arXiv:1109.6572 [hep-ex] (2011)`.

[52] ATLAS Collaboration, JHEP **12** (2010) 060.

[53] ATLAS Collaboration, ATLAS-CONF-2010-054 (2010).

[54] ATLAS Collaboration, Eur. Phys. J. **C71** (2011) 1577.

[55] ATLAS Collaboration, Phys. Lett. **B707** (2011) 418.

[56] G. Cowan, K. Cranmer, E. Gross, and O. Vitells, Eur. Phys. J. **C71** (2011) 1554.

[57] CDF Collaboration, Phys. Rev. Lett. **102** (2009) 221801.

[58] CDF Collaboration, Phys. Rev. Lett. **105** (2010) 081802.

[59] D0 Collaboration, Phys. Lett. **B693** (2010) 95–101.

[60] H. Baer, S. Kraml, A. Lessa, and S. Sekmen, JHEP **1002** (2010) 055.

[61] H. Baer, H. Raza, and Q. Shafi, `arXiv:1201.5668 [hep-ph] (2012)`.